energies

Article

# A Novel Multi-Phase Strategy for Optimizing $CO_2$ Utilization and Storage in an Oil Reservoir

**Jiangyuan Yao [1,*], Wanju Yuan [1], Xiaolong Peng [1], Zhuoheng Chen [1] and Yongan Gu [2]**

1 Geological Survey of Canada-Calgary, Natural Resources Canada, Calgary, AB T2L 2A7, Canada; wanju.yuan@nrcan-rncan.gc.ca (W.Y.); xiaolong.peng@nrcan-rncan.gc.ca (X.P.); zhuoheng.chen@nrcan-rncan.gc.ca (Z.C.)
2 Petroleum Technology Research Centre (PTRC), Petroleum Systems Engineering, Faculty of Engineering and Applied Science, University of Regina, Regina, SK S4S 0A2, Canada; peter.gu@uregina.ca
* Correspondence: jiangyuan.yao@nrcan-rncan.gc.ca; Tel.: +1-(306)-581-6830

**Abstract:** In this paper, an innovative multi-phase strategy is developed and numerically tested to optimize $CO_2$ utilization and storage in an oil reservoir to support low carbon transition. In the first phase, the water-alternating-gas (WAG) injection is conducted to simultaneously store $CO_2$ and produce crude oil in the reservoir from the respective injection and production wells. In the second phase, the injection and production wells are both shut in for some time to allow $CO_2$ and water to be stratigraphically separated. In the third phase, $CO_2$ is injected from the upper part of the reservoir above the separated water layer to displace water downwards, while fluids continue to be produced in the water-dominated zone from the lower part of the production well. Lastly, the production well is finally shut in when the produced gas–water ratio (GWR) reaches 95%, but $CO_2$ injection is kept until the reservoir pressure is close to the fracture pressure of its caprocks. The numerical simulations show that implementing the proposed multi-phase strategy doubles $CO_2$ storage in comparison to applying the WAG injection alone. In particular, 80% of the increased $CO_2$ is stored in the third phase due to the optimized perforation. In addition, the $CO_2$ injection rate in the last phase does not appear to affect the amount of $CO_2$ storage, while a higher $CO_2$ injection rate can reduce the $CO_2$ injection time and accelerate the $CO_2$ storage process. In the proposed strategy, we assume that the geothermal energy resources from the produced fluids can be utilized to offset some energy needs for the operation. The analysis of energy gain and consumption from the simulation found that at the early stage of the $CO_2$-WAG phase, the energy gain mostly comes from the produced oil. At the late stage of the $CO_2$-WAG phase and the subsequent phases, there is very little or even no energy gain from the produced oil. However, the geothermal energy of the produced water and $CO_2$ substantially compensate for the energy loss due to decreasing oil production. As a result, a net energy gain can be achieved from the proposed multi-phase strategy when geothermal energy extraction is incorporated. The new multi-phase strategy and numerical simulation provide insights for practical energy transition and $CO_2$ storage by converting a "to be depleted" oil reservoir to a $CO_2$ storage site and a geothermal energy producer while enhancing oil recovery.

**Keywords:** CCUS; WAG; multi-phase strategy; geothermal energy integration; energy sustainability



**Citation:** Yao, J.; Yuan, W.; Peng, X.; Chen, Z.; Gu, Y. A Novel Multi-Phase Strategy for Optimizing $CO_2$ Utilization and Storage in an Oil Reservoir. *Energies* **2023**, *16*, 5289. https://doi.org/10.3390/en16145289

Academic Editor: Devinder Mahajan

Received: 8 June 2023
Revised: 25 June 2023
Accepted: 8 July 2023
Published: 10 July 2023



## 1. Introduction

The use of carbon capture, utilization, and storage (CCUS) technology is crucial in mitigating climate change by reducing greenhouse gas emissions. In order to achieve the Government of Canada's target of net-zero emissions by 2050, the CCUS technique must offset 395 Mt of $CO_2$ per year [1]. Alberta, being the province with the highest oil and gas production in Canada, emitted 273 Mt of greenhouse gases into the atmosphere in 2020, which accounted for over one-third of the country's total emissions [2]. Therefore, it is essential to decarbonize Alberta to achieve the Canadian Government's carbon reduction goal. The oil and gas sector must reduce its $CO_2$ emissions from 182 Mt/year in 2021 to 110 Mt/year in 2030 to stay on Canada's greenhouse gas emissions pathway to 2030 [3]. This will require a significant portion of the reduction to come from the implementation of the CCUS technology. Currently, a meager 5 Mt of $CO_2$ is sequestrated annually in Canada, a considerable disparity from the decarbonization ambition outlined by the Government [3]. To remove $CO_2$ emissions from the atmosphere, there is an urgent need to develop a CCUS technology that is technically effective and economically viable.

Several researchers have conducted extensive studies on the integration of $CO_2$-based enhanced oil recovery ($CO_2$-EOR) with $CO_2$ storage [4]. Kamali et al. experimentally and numerically studied the co-optimizing of $CO_2$ storage and $CO_2$-EOR. It has been found that near-miscible displacement yields the highest $CO_2$ storage efficiency and the gravity effects in the near-miscible and miscible displacement cannot be neglected [5]. It has been claimed by Ahmadi et al. that there exists an optimum injection rate for the $CO_2$ injection process based on the numerical studies [6]. Bello et al. investigated the role of $CO_2$ foam EOR in the reduction in carbon emissions and suggested that the approach of generating $CO_2$ foams can boost financial incentives, help to lower carbon emissions, and produce the crude oil in a more sustainable way [7]. Depleted oil reservoirs offer significant advantages over other $CO_2$ storage sites, such as aquifers and deep oceans, due to lower capital costs and more economic incentives from oil production [8–11]. Furthermore, $CO_2$-EOR techniques have been utilized for approximately half a century in the oil industry [12,13], resulting in more comprehensive investigations of the processes of using $CO_2$-EOR techniques for $CO_2$ storage in depleted oil reservoirs than those in other sites [14,15]. Among the $CO_2$-EOR techniques, $CO_2$-based water-alternating-gas ($CO_2$-WAG) has been one of the most successfully practiced techniques, as it improves the sweep efficiency and delays $CO_2$ breakthrough [16,17].

Numerous studies have been carried out in recent years to explore the use of supercritical $CO_2$ as an alternative to water in enhanced geothermal systems (EGS), which enable the combination of $CO_2$ storage and geothermal energy extraction [18]. The advantages of geothermal energy, including continuous exploitation and independence from weather conditions, make it a promising renewable energy source to supplement fossil fuels [19–21]. Supercritical $CO_2$ has several advantages over water for geothermal energy exploitation, such as extremely low viscosity and high heat capacity, which lead to a high injectivity and heat mining rate [22–24]. Additionally, it has a larger compressibility and expansivity than water, which can reduce the parasitic power consumption in the fluid circulation system due to an increased buoyancy force and thermosiphon effect [18,25]. Most importantly, after geothermal exploitation is completed, a significant amount of $CO_2$ can be stored in the reservoir [26]. Brown (2000) was the first to propose the concept of $CO_2$-EGS using supercritical $CO_2$, suggesting that it could be used as a heat transmission fluid for geothermal energy extraction in hot dry rocks [18]. However, the potential risks associated with induced earthquakes and $CO_2$ leakage must be carefully considered. Hsieh et al. discussed the heat transfer between supercritical $CO_2$ and the surrounding heat in an upward flow vertical tube with silica-based porous media [27]. Randolph et al. (2011) proposed the use of supercritical $CO_2$ as a work fluid in geothermal energy extraction in high porosity and high permeability formations, which is referred to as $CO_2$-based plume geothermal (CPG) technology [28]. More studies have since been conducted on CPG systems, and some researchers agree that they can be more efficient than water-based systems due to the lower viscosity and higher flow rate of supercritical $CO_2$ [18,29]. Garapati et al. found that the heterogeneity of the reservoir can significantly affect the performance of $CO_2$-CPG systems [30], while Benjamin et al. concluded that $CO_2$ is an ideal fluid for CPG systems in shallow reservoirs [31].

The preceding statements indicate that employing $CO_2$ for EOR processes and geothermal energy extraction is an effective approach for mitigating greenhouse gas emissions by sequestering $CO_2$ in underground reservoirs on a permanent basis. However, it is essential to acknowledge their limitations. Specifically, when $CO_2$-EOR procedures are completed, oil reservoirs still have significant potential for $CO_2$ storage [6]. Nonetheless, the lack of economic incentives in the oil industry could impede the use of existing wells for converting depleted oil reservoirs into $CO_2$ storage sites. Furthermore, the high capital costs of drilling new wells and constructing expensive facilities for geothermal energy exploitation are major obstacles to the development of $CO_2$ applications in geothermal energy extraction [27]. The novelty of this study lies in the innovative multi-phase strategy it proposes that integrates $CO_2$-EOR and geothermal energy extraction processes to overcome the above-mentioned obstacles and maximize $CO_2$ storage capacity in an oil reservoir. This proposed strategy can be applied to a "to be depleted" oil reservoir for $CO_2$ storage and geothermal production, while achieving EOR, which can help motivate the oil industry to conduct CCUS projects with reduced economic burdens by making use of the existing infrastructure and receiving carbon credits. By comparing the amount of $CO_2$ storage achieved by applying the multi-phase strategy with that of $CO_2$-EOR alone, the effectiveness and efficiency of the multi-phase strategy in $CO_2$ storage have been validated. Additionally, an energy analysis has been conducted, concluding that positive energy gains can be achieved, and energy sustainability can be attained when implementing the multi-phase strategy.

## 2. Methods

### *2.1. The Multi-Phase Strategy*

Figure 1 shows the schematic diagram of the multi-phase strategy proposed in this paper. In the first phase, both injection and production wells are fully opened. The water-alternating-gas (WAG) injection is conducted, during which the water and $CO_2$ are alternatingly injected from an injection well and the crude oil is produced from a production well, while part of the injected $CO_2$ remains in the reservoir. In the second phase, both the injection and production wells are shut in for approximately one year once the water cut is larger than 95% so that the injected $CO_2$ and water can be stratigraphically separated by buoyance force. In the third phase, an optimized and well thought out perforation plan is applied, i.e., only one-tenth on the top of the injection well and one-tenth on the bottom of the production well are reopened. Then $CO_2$ is injected from the top of the injection well to push the water in the reservoir downward to be produced from the production well. The production well is shut in again when the volume ratio of produced $CO_2$ to the total volume of the produced fluids under reservoir conditions is larger than 95%. Meanwhile, the injection well is kept open. $CO_2$ is continuously injected and stored in the reservoir until the reservoir pressure is close to the fracture pressure of its caprock, which is described in Section 2.2. By doing so, $CO_2$ is utilized to recover oil and then stored in the oil reservoir by using the existing wells. As a result, the oil reservoir is converted into $CO_2$ storage site at a minimum cost in addition to geothermal heat energy extraction that could potentially be used to offset the greenhouse gas (GHG) emissions from the operation site.

### *2.2. Description of Geological Model*

A homogeneous 3-D geological model is constructed to evaluate the effects on $CO_2$ storage capacity when the multi-phase strategy is applied. The porosity and permeability of the geological model are 10% and 1 Darcy, respectively, which are close to the values in Nisku carbonate formation in Pembina Oilfield, Alberta, Canada [32]. The respective length, width, and thickness of the geological model are 1200 m, 1200 m, and 100 m. The depth of the top of the geological model is 2800 m. The geological model is discretized to 9000 grids and the size of each grid is 40 m in length, 40 m in width, and 1 m in thickness. By checking the data of Nisku carbonate formation reported by Chevron Standard Limited [32], the initial water saturation ($S_{iw}$) and irreducible oil saturation ($S_{oi}$) of the geological model are set to be 30% and 25%, respectively. The initial reservoir temperature and pressure are 90 °C and 25 MPa, respectively. The reservoir fracture pressure is set to be 30 MPa, which is 5 MPa higher than the initial reservoir pressure. More detailed data of the geological model are listed in Table 1.

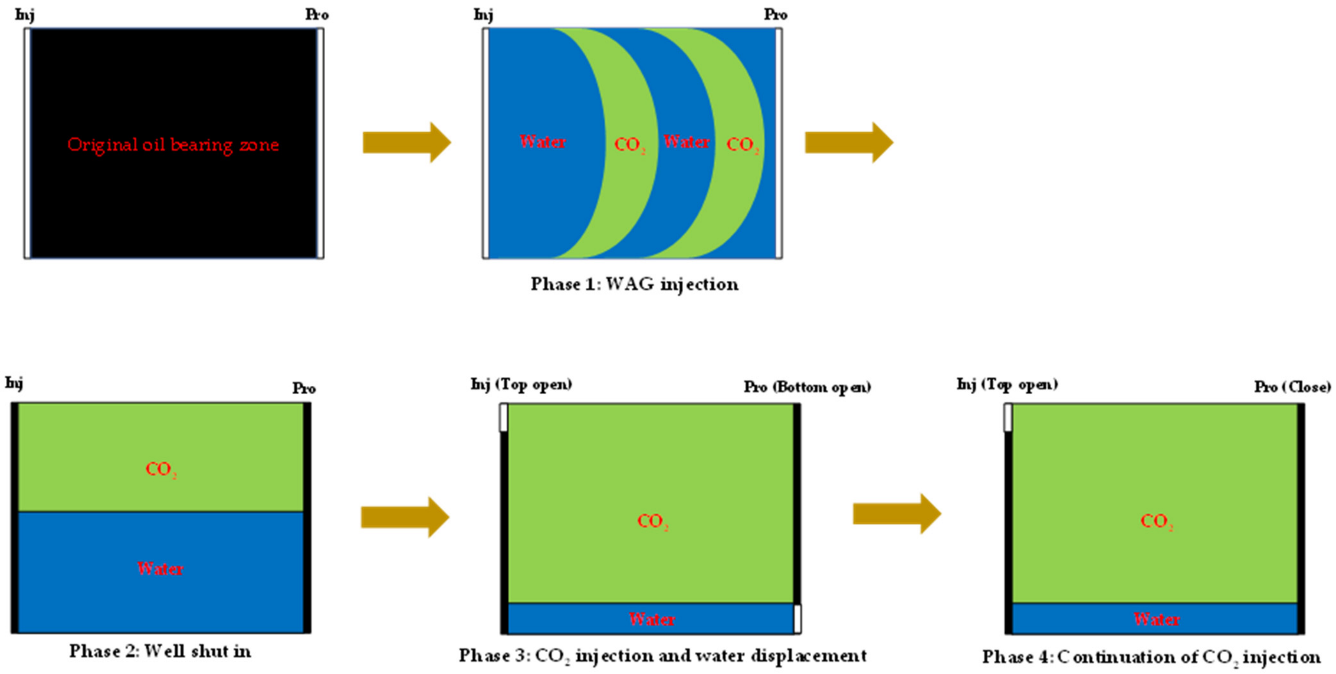


**Figure 1.** The schematic diagram of the multi-phase strategy for $CO_2$ utilization and storage. Phase 1: both the injector and producer are fully opened; Phase 2: both the injector and producer are closed; Phase 3: only the top of the injector and bottom of producer are opened; Phase 4: the top of the injector is kept open, while the producer is closed.

**Table 1.** The properties of the homogenous geological model.

| Size | 1200 m × 1200 m × 100 m |
|---|---|
| Depth | 2800 m |
| Pressure | 25 MPa |
| Temperature | 95 °C |
| Wettability | oil wet |
| Porosity | 10% |
| Permeability | 1.5 D |
| Initial oil saturation | 70% |
| Irreducible oil saturation | 25% |
| Pore volume | $1.44 \times 10^7$ m$^3$ |
| OOIP | $1.01 \times 10^7$ m$^3$ |

### *2.3. Numerical Simulations*

The compositions and properties of the crude oil used in this numerical simulation study are listed in Table 2a,b, respectively. The data are referred from Yao's work in 2022 [33]. A total of fifteen scenarios, which are listed in Table 3, were simulated by using the GEM and STARS modules of the CMG software. More specifically, the GEM module is used as the simulator to investigate $CO_2$ utilization and storage efficiencies in all scenarios. The STARS module is used to simulate Scenarios #2 and #11 to obtain the temperatures of the produced fluids for energy analysis. A five-spot well pattern is applied in all numerical simulations. The only injection well is in the centre of the oil reservoir, and four production wells are in the four corners of the geological model. The production pressures in all scenarios are set the same as 25 MPa in order to make sure the injected $CO_2$ can be miscible with the crude oil in place for a better performance of $CO_2$-WAG injection process since the minimum miscibility pressure between $CO_2$ and the crude oil is 15 MPa. In Scenarios #1, 2, and 3, only the $CO_2$-WAG injection is conducted and simulated. In these scenarios, the water and $CO_2$ are alternatingly injected into the reservoir year by year; however, the water–$CO_2$ slug size ratio are different. In Scenario #1, the water and $CO_2$ injection rates are 15,000 $m^3$/year and 5000 $m^3$/year under the reservoir conditions, respectively. In Scenarios #2 and #3, the water injection rates are the same as that in Scenario #1, while the respective $CO_2$ injection rates at the reservoir conditions are 15,000 $m^3$/year and 45,000 $m^3$/year. Thus, the water–$CO_2$ slug size ratios in Scenarios #1, 2, and 3 under the reservoir conditions are 3:1, 1:1, and 1:3, respectively. Scenarios #4–15 simulate the entire four phases of the multi-phase strategy to study the effects of $CO_2$ injection rate in Phase 3 and Phase 4 on $CO_2$ utilization and storage. More specifically, the water slug sizes, $CO_2$ slug sizes, and water–$CO_2$ slug ratios of the WAG injection phase in Scenarios #4–7 remain the same, which are 15,000 $m^3$/year, 5000 $m^3$/year, and 3:1 under the reservoir conditions, respectively. The differences of these scenarios are $CO_2$ injection rates in Phases 3 and 4, which are 5000 $m^3$/year, 10,000 $m^3$/year, 15,000 $m^3$/year, and 20,000 $m^3$/year under reservoir conditions in Scenarios #4, 5, 6, and 7, respectively. Scenarios #8–11 and #12–15 have the same $CO_2$ injection rates in Phases 3 and 4 as Scenarios #4–7. However, the water–$CO_2$ slug ratios in the series of Scenarios #8–11 and #12–15 are different, which are 1:1 and 1:3 under the reservoir conditions, respectively.

**Table 2.** (a). The compositions of the crude oil used in the numerical simulation [33]. (b). The crude oil properties at the atmospheric pressure and the temperature of 20 °C [33].

**(a)**

| Carbon No. | mol.% | Carbon No. | mol.% |
|---|---|---|---|
| $C_1$ | 0.00 | $C_{31}$ | 0.88 |
| $C_2$ | 0.00 | $C_{32}$ | 0.77 |
| $C_3$ | 0.00 | $C_{33}$ | 0.70 |
| $C_4$ | 0.09 | $C_{34}$ | 0.66 |
| $C_5$ | 1.66 | $C_{35}$ | 0.64 |
| $C_6$ | 3.30 | $C_{36}$ | 0.55 |
| $C_7$ | 8.37 | $C_{37}$ | 0.48 |
| $C_8$ | 7.46 | $C_{38}$ | 0.46 |
| $C_9$ | 10.05 | $C_{39}$ | 0.44 |
| $C_{10}$ | 5.33 | $C_{40}$ | 0.40 |
| $C_{11}$ | 5.22 | $C_{41}$ | 0.35 |
| $C_{12}$ | 5.51 | $C_{42}$ | 0.33 |
| $C_{13}$ | 4.12 | $C_{43}$ | 0.30 |
| $C_{14}$ | 4.08 | $C_{44}$ | 0.29 |
| $C_{15}$ | 3.80 | $C_{45}$ | 0.28 |
| $C_{16}$ | 3.38 | $C_{46}$ | 0.26 |
| $C_{17}$ | 3.38 | $C_{47}$ | 0.25 |
| $C_{18}$ | 3.04 | $C_{48}$ | 0.23 |
| $C_{19}$ | 2.70 | $C_{49}$ | 0.20 |
| $C_{20}$ | 2.32 | $C_{50}$ | 0.20 |
| $C_{21}$ | 2.06 | $C_{51}$ | 0.20 |
| $C_{22}$ | 1.80 | $C_{52}$ | 0.17 |
| $C_{23}$ | 1.64 | $C_{53}$ | 0.15 |

**Table 2.** *Cont.*

| | | | |
|---|---|---|---|
| $C_{24}$ | 1.53 | $C_{54}$ | 0.15 |
| $C_{25}$ | 1.49 | $C_{55}$ | 0.16 |
| $C_{26}$ | 1.38 | $C_{56}$ | 0.14 |
| $C_{27}$ | 1.27 | $C_{57}$ | 0.13 |
| $C_{28}$ | 1.18 | $C_{58}$ | 0.12 |
| $C_{29}$ | 1.07 | $C_{59}$ | 0.11 |
| $C_{30}$ | 0.96 | $C_{60+}$ | 1.81 |
| | | Total | 100.00 |

**(b)**

| | |
|---|---|
| Molecular weight | 256.0 g/mol |
| Density | 0.829 g/cm$^3$ |
| Specific gravity (SG) | 0.829 |
| Viscosity | 8.7 cP |
| Minimal miscibility pressure with $CO_2$ | 15 MPa |

**Table 3.** The design of each scenario that is numerically simulated in this study, in which volume measures are in reservoir condition.

| **Scenario No.** | **WAG Injection Phase** | | **Phases 3 and 4** | **Simulator** | **Note** |
|---|---|---|---|---|---|
| | **$CO_2$ Injection Rate** | **Water–$CO_2$ Slug Size Ratio** | **$CO_2$ Injection Rate** | | |
| | **(m$^3$/d)** | **(m$^3$/m$^3$)** | **(m$^3$/d)** | | |
| 1 | 5000 | 3:1 | N/A | GEM | Only the WAG injection phase is simulated |
| 2 | 15,000 | 1:1 | N/A | GEM and STARS | |
| 3 | 45,000 | 1:3 | N/A | GEM | |
| 4 | 5000 | 3:1 | 5000 | GEM | All phases of the multi-phase strategy are simulated |
| 5 | 5000 | | 10,000 | GEM | |
| 6 | 5000 | | 15,000 | GEM | |
| 7 | 5000 | | 20,000 | GEM | |
| 8 | 15,000 | 1:1 | 5000 | GEM | |
| 9 | 15,000 | | 10,000 | GEM | |
| 10 | 15,000 | | 15,000 | GEM | |
| 11 | 15,000 | | 20,000 | GEM and STARS | |
| 12 | 45,000 | 1:3 | 5000 | GEM | |
| 13 | 45,000 | | 10,000 | GEM | |
| 14 | 45,000 | | 15,000 | GEM | |
| 15 | 45,000 | | 20,000 | GEM | |

*2.4. Integrated $CO_2$-EOR Process with Geothermal Energy Extraction*

The schematic diagram of $CO_2$-EOR process with integration of geothermal energy extraction is depicted in Figure 2. First, we assume that $CO_2$ is captured in a powerplant. Then the captured $CO_2$ at a known pressure $P_1$ and temperature $T_1$ is compressed by

Compressor #1 to an elevated pressure $P_2$ and temperature $T_2$ then transported in a 200 km long pipeline to the oilfield. On the oilfield site, the transported $CO_2$ at a pressure $P_3$ and temperature $T_3$ is re-compressed to the injection pressure $P_4$ by Compressor #2. On the other hand, water at the original pressure $P_5$ and temperature $T_5$ is also transported and compressed to the pressure $P_6$. Then the water and $CO_2$ are injected into the reservoir based on the scheduled water and $CO_2$ slug sizes and the water–$CO_2$ slug size ratio. It is assumed that the water source is close to the oilfield; therefore, the water transportation is neglected in this analysis. On the production end, the produced oil, $CO_2$, and water at the pressures and temperatures of $P_{oil}$, $P_{CO2}$, $P_{water}$ and $T_{oil}$, $T_{CO2}$, $T_{water}$ go through a heat exchanger and all leave at the ambient pressure and temperature so that the geothermal energies carried by the production fluids are extracted by the heat exchanger. Then the produced oil, $CO_2$, and water at the ambient pressure and temperature are separated in a surface separator. Afterwards, the produced oil is pumped to a refinery for further processing, the produced $CO_2$ and water is compressed by Compressor #3 and the water pump, respectively, and reinjected into the reservoir to produce oil. All the pressures and temperatures mentioned in this process are given in Table 4.

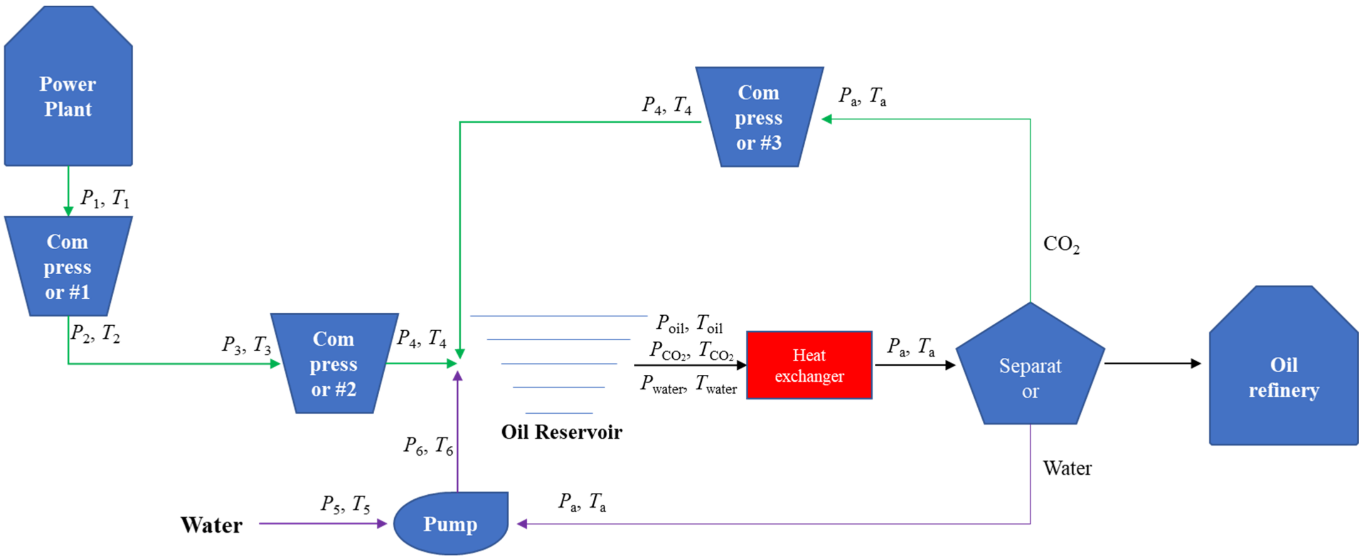


**Figure 2.** The schematic diagram of $CO_2$-EOR system integrated with geothermal energy extraction.

**Table 4.** The pressures and temperatures in different parts of $CO_2$-EOR system integrated with geothermal energy extraction.

| | Pressure | Temperature |
|---|---|---|
| | bar | °C |
| Pressure and temperature of captured $CO_2$ ($P_1$, $T_1$) | 1 | 20 |
| $CO_2$ pressure and temperature after Compressor #1 ($P_2$, $T_2$) | 80 | 20 |
| $CO_2$ pressure and temperature before Compressor #2 ($P_3$, $T_3$) | 50 | 20 |
| $CO_2$ pressure and temperature after Compressor #2 ($P_4$, $T_4$) | Obtained from simulation | 20 |

**Table 4.** *Cont.*

| | Pressure | Temperature |
|---|---|---|
| | bar | °C |
| Water pressure and temperature before water pump ($P_5$, $T_5$) | 1 | 20 |
| Water pressure and temperature after water pump ($P_6$, $T_6$) | Obtained from simulation | 20 |
| Pressure and temperature of produced fluids ($P_{oil}$, $P_{CO_2}$, $P_{water}$ and $T_{oil}$, $T_{CO_2}$ and $T_{water}$) | 180 | Obtained from simulation |
| $CO_2$ pressure and temperature before Compressor #3 | 1 | 20 |
| $CO_2$ pressure and temperature after Compressor #3 | Same as $P_4$ | 20 |
| water pressure and temperature before reinjection | 1 | 20 |
| water pressure and temperature after reinjection | Same as $P_6$ | 20 |

In the entire process, the energy gains are from two sources, which are the energy of the produced oil and geothermal energies from the produced oil, $CO_2$, and water. Accordingly, the major energy consumption parts are the powerplant for $CO_2$ capture, the compressors and water pump, and the surface separator. The energy consumption for oil transport to the refinery is not accounted for in this study. The methods to calculate the energy gains and consumptions are described in the following section of Results and Discussions.

## 3. Results and Discussions

### *3.1. Comparison of the WAG Injection Processes with Different Water–$CO_2$ Slug Size Ratios*

Scenarios #1–3 are simulated to show and compare the performances of the WAG injection processes with different water–$CO_2$ slug ratios of 3:1, 1:1, and 1:3. The cumulative oil production and final oil recovery factor (ORF) are displayed in Figure 3a,b, respectively. It can be seen from these figures that Scenario #2 with the medium water–$CO_2$ slug ratio of 1:1 has the maximum oil recovery in comparison to Scenarios #1 and #3, which have the highest and lowest water–$CO_2$ slug ratios of 3:1 and 1:3, respectively. This indicates that there is an optimum water–$CO_2$ slug ratio. This is because the injected $CO_2$ is much less viscous than the injected water and the reservoir oil. Too much injected $CO_2$ can cause a severe viscous fingering, thus reducing the sweep efficiency of $CO_2$ and leading to low oil recovery. On the other hand, if the amount of injected $CO_2$ is too little, there would not be enough $CO_2$ to be used to replace the crude oil from the reservoir by swelling and diluting the crude oil [34]. It can also be found from Figure 3a that most of the oil in the reservoir is produced during the first two cycles of the WAG injection in all the three Scenarios, and very little oil can be recovered in the following cycles. This means that the existing wells that have been used for the WAG injection process can be converted into $CO_2$ injection wells for $CO_2$ storage after the first few cycles of the WAG injection. Figure 4 shows the comparison of the $CO_2$ utilization ratios of the three scenarios in the years of $CO_2$ injection. In this paper, the $CO_2$ utilization ratio is defined as the volume of oil in standard conditions recovered by the unit mass of injected $CO_2$ and the unit of this quantity is $m^3/t$. It can be seen from Figure 4 that Scenario #2, which has the water–$CO_2$ slug size ratio of 1:1, has the highest $CO_2$ utilization ratio, which means that the injected $CO_2$ has a higher efficiency in oil recovery as compared to those in Scenarios #1 and #3. In other words, more oil can be produced from the WAG injection process if the water–$CO_2$ slug size ratio of 1:1 is used in $CO_2$-EOR practice for the reservoir condition in this study.

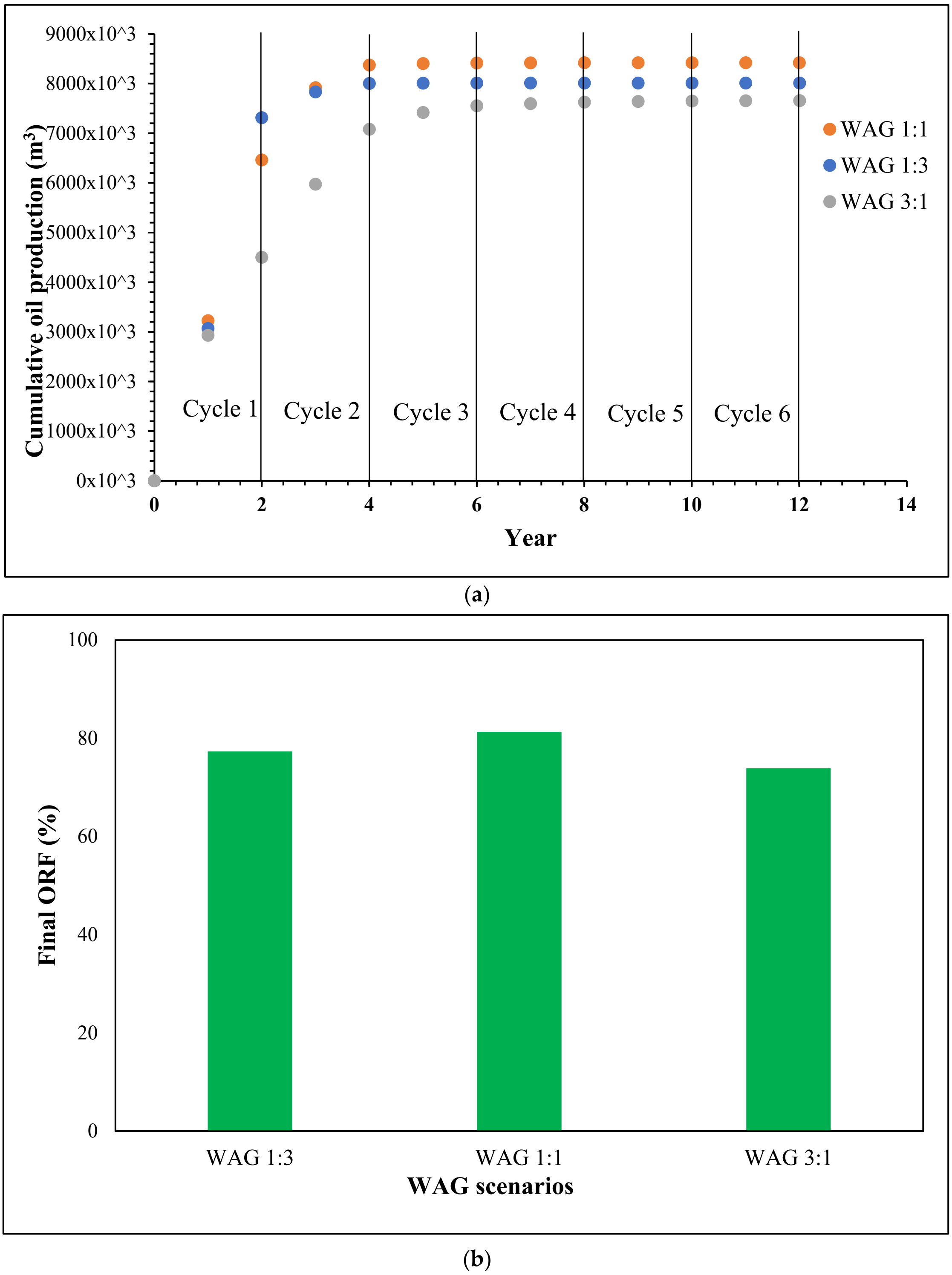


**Figure 3.** The comparisons of (**a**) cumulative oil production and (**b**) the final oil recovery factor in different WAG injection processes with different water–$CO_2$ slug ratios of 3:1, 1:1, and 1:3.

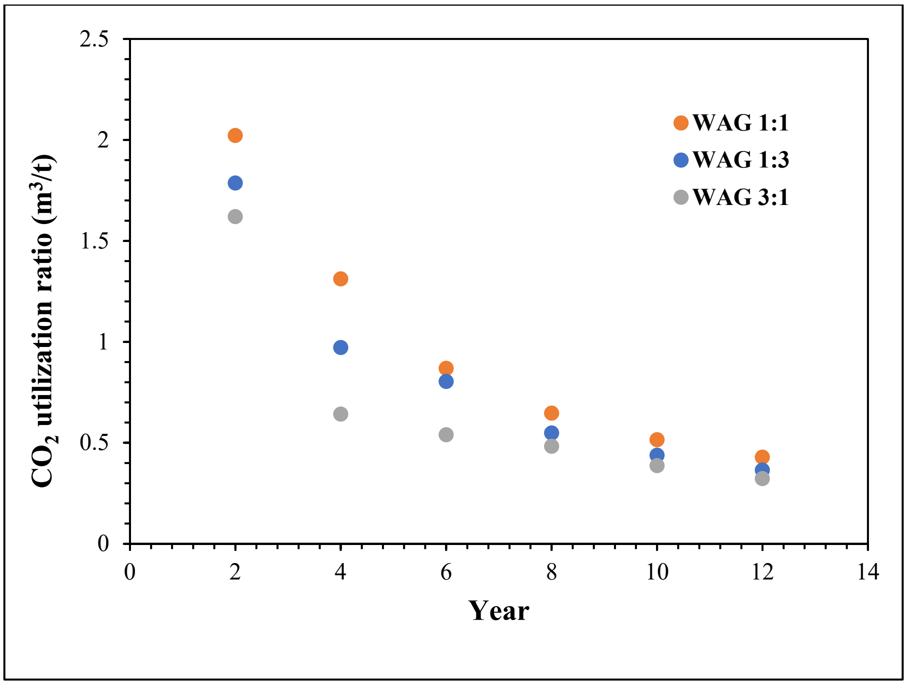


**Figure 4.** The comparison of $CO_2$ utilization ratio in different WAG injection processes with different water–$CO_2$ slug ratios of 3:1, 1:1, and 1:3.

From the results of the simulation, it seems that there is an optimum water–$CO_2$ slug size ratio for $CO_2$ utilization in the WAG injection process. Either a too large or too small water–$CO_2$ slug size ratio could lead to a low $CO_2$ utilization efficiency in the WAG injection process.

### *3.2. $CO_2$ Storage Efficiency*

The comparison of the amount of $CO_2$ stored in Scenarios #2 and #11 is shown in Figure 5a. Scenarios #2 and #11 have the same water and $CO_2$ injection rates, water–$CO_2$ slug size ratio, and production pressure in the WAG injection phase. Scenario #11 simulates the entire multi-phase strategy, while Scenario #2 only simulates the WAG injection phase. It can be seen from Figure 5a that the amount of $CO_2$ stored in Scenario #2 is about a half of that in Scenario #11. Scenarios #7, #11, and #15 were selected as examples to demonstrate the amount of $CO_2$ storage in and after the WAG injection phase, which is shown in Figure 5b. It can quickly be found from this figure that there is a large amount of $CO_2$ that can be stored after the WAG injection phase no matter what the water–$CO_2$ slug size ratio is. This suggests that the wells can still be applied to store and sequestrate $CO_2$ by employing the proposed multi-phase strategy when the WAG injection process is finished. By doing so, on the one hand, the life expectancy of the wells used in the WAG injection process are extended. On the other hand, the depleted oil reservoir after the WAG injection process can be converted to a $CO_2$ storage site by using existing wells to offset GHG emission, which can largely save the cost to realize the $CO_2$ storage potential of the depleted oil reservoir.

Figure 6 demonstrates the proportion of $CO_2$ stored in each phase. It can be found from this figure that half the amount of $CO_2$ storage is attributed to the first phase. The third and last phases in total contribute to the other half of $CO_2$ storage. In particular, 37% of $CO_2$ is stored in the third phase, in which an optimized well perforation and $CO_2$ injection are performed. In other words, the amount of $CO_2$ storage can be doubled by applying the multi-phase strategy in comparison to the WAG process alone. More specifically, almost 80% of the increased $CO_2$ storage is from Phase 3. These findings imply two views, first, the proposed multi-phase strategy is proven to be an effective way to store $CO_2$ by converting a depleted oil reservoir into a $CO_2$ storage site. Second, the optimized well perforation is the key element of the multi-phase strategy for the increase in $CO_2$ storage.

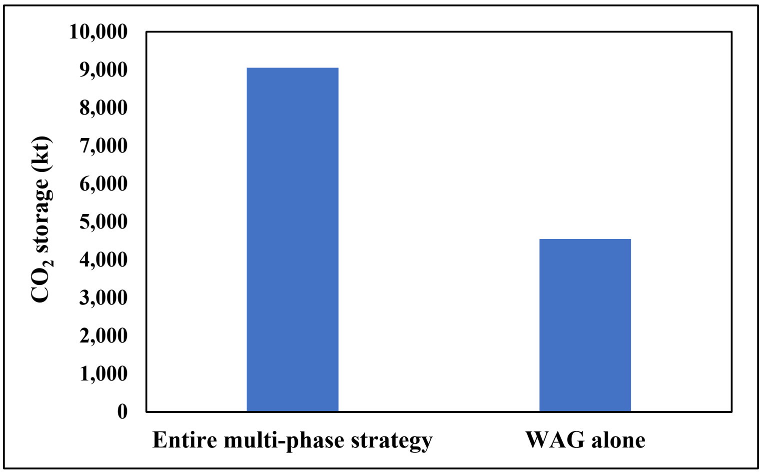


(**a**)

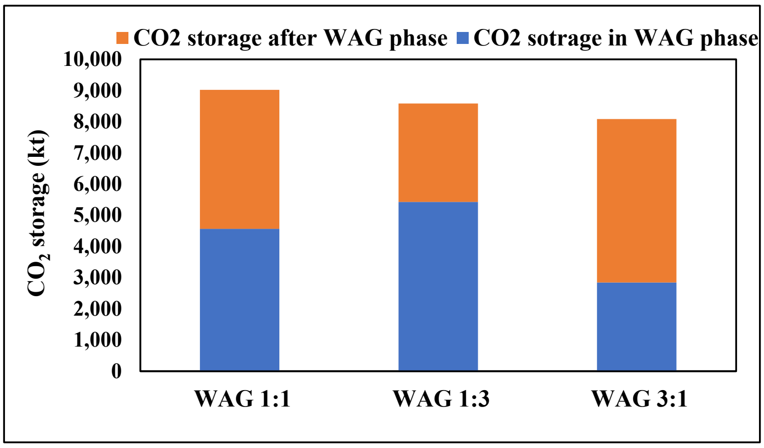


(**b**)

**Figure 5.** The comparisons of the total $CO_2$ storage (**a**) between Scenario #11 in which the entire multi-phase strategy is simulated and Scenario #2 in which only the WAG phase is simulated; and (**b**) between Scenarios #11, 15, and 7, which have different water–$CO_2$ slug ratios of 1:1, 1:3, and 3:1.

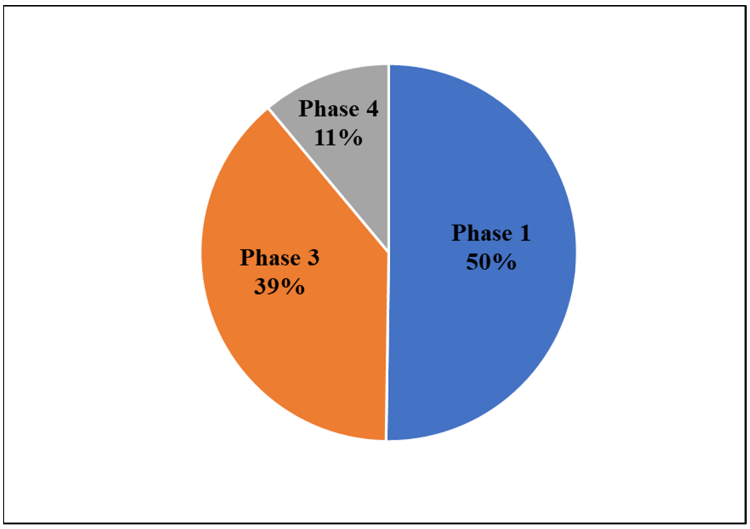


**Figure 6.** The proportions of $CO_2$ stored in different phases of the multi-phase strategy.

### 3.3. The Effects of $CO_2$ Injection Rate

Figure 7 shows the $CO_2$ storage efficiency vs. the $CO_2$ injection rate in Phase 3 and 4 at different water–$CO_2$ slug size ratios. In this paper, $CO_2$ storage efficiency is defined as the ratio of the total volume of $CO_2$ stored in the reservoir conditions to the volume of the pore space occupied by original hydrocarbons. It can be seen from this figure that the $CO_2$ storage efficiencies of the scenarios with the water–$CO_2$ injection rate of 1:1 are higher than those of the scenarios with the water–$CO_2$ slug size ratio of 3:1 and 1:3. This is because the scenario with the water–$CO_2$ slug size ratio of 1:1 has a higher oil recovery in the WAG injection phase than those from applying other slug size ratios examined, which has been explained in Section 3.1. As a result, more pore spaces that are originally occupied by oil are available for $CO_2$ storage in the scenario with the water–$CO_2$ slug size ratio of 1:1 than those in the scenarios with the water–$CO_2$ slug size ratios of 3:1 and 1:3, which leads to a higher $CO_2$ storage efficiency.

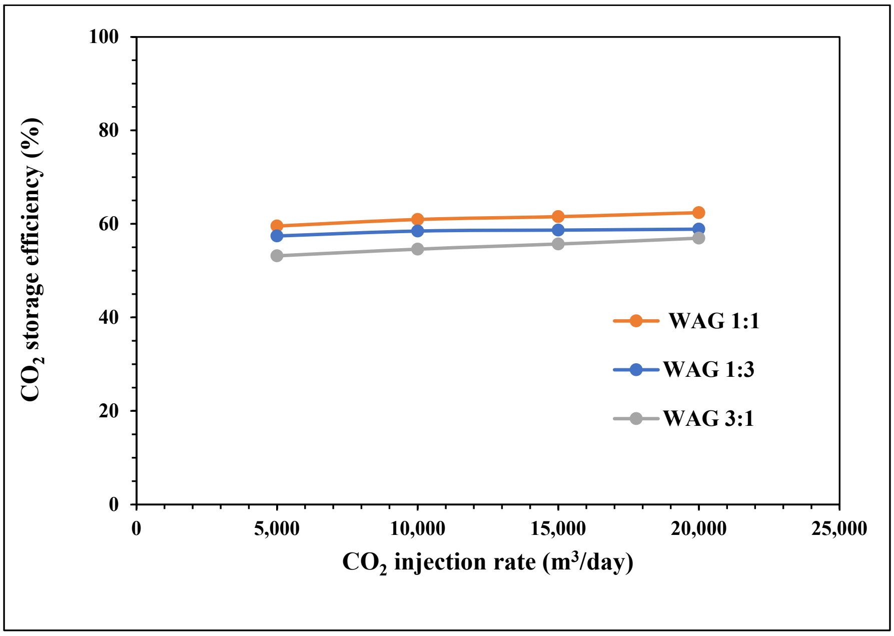


**Figure 7.** The comparison of $CO_2$ storage efficiency between the scenarios with different water–$CO_2$ slug size ratios at different $CO_2$ injection rates in Phase 3 and 4.

It is shown in Figure 7 that $CO_2$ storage efficiency is not affected by $CO_2$ injection pressure in Phase 3 and 4 for all scenarios, no matter what the water–$CO_2$ slug ratios are. This indicates that the $CO_2$ injection rate does not appreciably affect the final $CO_2$ storage efficiency in the range of this simulation study. However, a higher injection rate can lead to a short injection time. This finding denotes that the implementation of the multi-phase strategy for $CO_2$ storage can be accelerated by applying a high injection rate since it will not sacrifice the $CO_2$ storage efficiency, which is significantly useful to reach the zero emissions goal in 2050 set by the Government of Canada.

### 3.4. Energy Analysis

#### 3.4.1. Calculations of Energy Gains

As stated in Section 2.4, the energy gain comes from the produced oil and the geothermal energy extracted from the produced fluids. The energy gain from the produced oil is obtained by calculating its lower heating value (LHV), which is generally assumed to be the chemical exergy of the crude oil [35,36]. The following correlation is used to calculate the LHV of the produced oil in this study [35].

$$\mathrm{LHV} = 55.5 - 14.4\ \mathrm{SG} \tag{1}$$

where LHV is the lower heating value of the produced oil, MJ/kg; and SG is the specific gravity of the produced oil, which is given in Table 2b. The geothermal energies extracted from the produced fluids (oil, $CO_2$, and water) are their enthalpy differences before and after the heat exchanger times the efficiency of the heat exchanger, which can be expressed as:

$$E_{\mathrm{H}}^{\mathrm{CO_2}} = \eta_{\mathrm{HE}} \Delta H_{\mathrm{CO_2}} = \eta_{\mathrm{HE}} \left( H_{\mathrm{CO_2}} \left( P_{\mathrm{CO_2}},\ T_{\mathrm{CO_2}} \right) - H_{\mathrm{CO_2}} \left( P_{\mathrm{a}},\ T_{\mathrm{a}} \right) \right) \tag{2}$$

$$E_{\mathrm{H}}^{\mathrm{oil}} = \eta_{\mathrm{HE}} \Delta H_{\mathrm{oil}} = \eta_{\mathrm{HE}} \left( H_{\mathrm{oil}} \left( P_{\mathrm{oil}},\ T_{\mathrm{oil}} \right) - H_{\mathrm{oil}} \left( P_{\mathrm{a}},\ T_{\mathrm{a}} \right) \right) \tag{3}$$

$$E_{\mathrm{H}}^{\mathrm{water}} = \eta_{\mathrm{HE}} \Delta H_{\mathrm{water}} = \eta_{\mathrm{HE}} \left( H_{\mathrm{water}} \left( P_{\mathrm{water}},\ T_{\mathrm{water}} \right) - H_{\mathrm{water}} \left( P_{\mathrm{a}},\ T_{\mathrm{a}} \right) \right) \tag{4}$$

where $E_{\mathrm{H}}^{\mathrm{CO_2}}$, $E_{\mathrm{H}}^{\mathrm{oil}}$, and $E_{\mathrm{H}}^{\mathrm{water}}$ are the geothermal energies recovered from the produced $CO_2$, oil, and water, respectively, MJ; $\eta_{\mathrm{HE}}$ is the efficiency of the heat exchanger; $\Delta H_{\mathrm{CO_2}}$, $\Delta H_{\mathrm{oil}}$, and $\Delta H_{\mathrm{water}}$ are the enthalpy differences of the respective produced $CO_2$, oil, and water before and after the heat exchanger, MJ; $H_{\mathrm{CO_2}}$, $H_{\mathrm{oil}}$, and $H_{\mathrm{water}}$ are the enthalpies of $CO_2$, oil, and water at a known pressure and temperature, MJ, which can be obtained by using the Winprop module of the CMG software. $T_{\mathrm{CO_2}}$, $T_{\mathrm{oil}}$, and $T_{\mathrm{water}}$ are the temperatures of the produced fluids, K; and $P_{\mathrm{a}}$ is the atmospheric pressure, Pa.

### 3.4.2. Calculations of Energy Consumptions

$CO_2$ capture consumes large amounts of energy [37]. The average energy consumption for separating $CO_2$ from flue gas by using the current predominant carbon capture technology of the monoethanolamine (MEA) method is equal to $E_{\mathrm{cap}}$ = 4000 kJ/kg [36], which is used in this study.

The method to calculate the energy consumptions of the transport of $CO_2$, the injection and reinjection of $CO_2$, and water is to calculate the enthalpy differences before and after the compressors or water pump. For example, as for $CO_2$ transport, the amount of energy consumed in Compressor #1 can be expressed as:

$$W_{\mathrm{comp1}} = \frac{H_{\mathrm{CO_2}}(P_2,\ T_2) - H_{\mathrm{CO_2}}(P_1,\ T_1)}{\eta_{\mathrm{comp1}}} \tag{5}$$

Similarly, the energies consumed in Compressors #2 and #3 for $CO_2$ injection and reinjection can be expressed as:

$$W_{\mathrm{comp2}} = \frac{H_{\mathrm{CO_2}}(P_4,\ T_4) - H_{\mathrm{CO_2}}(P_3,\ T_3)}{\eta_{\mathrm{comp2}}} \tag{6}$$

and

$$W_{\mathrm{comp3}} = \frac{H_{\mathrm{CO_2}}(P_4,\ T_4) - H_{\mathrm{CO_2}}(P_{\mathrm{a}},\ T_{\mathrm{a}})}{\eta_{\mathrm{comp3}}} \tag{7}$$

The energies consumed in the water pump for water injection and reinjection can be expressed as:

$$W_{\mathrm{pump}} = \frac{H_{\mathrm{water}}(P_6,\ T_6) - H_{\mathrm{water}}(P_{\mathrm{a}},\ T_{\mathrm{a}})}{\eta_{\mathrm{pump}}} \tag{8}$$

where $W_{\mathrm{comp1}}$, $W_{\mathrm{comp2}}$, $W_{\mathrm{comp3}}$, and $W_{\mathrm{pump}}$ are the energies consumed in Compressors #1, 2, and 3 and the water pump, respectively; $\eta_{\mathrm{comp1}}$, $\eta_{\mathrm{comp2}}$, $\eta_{\mathrm{comp3}}$, and $\eta_{\mathrm{pump}}$ are the respective work efficiencies of Compressors #1, 2, 3, and the water pump. In this study, the efficiency of the compressors is 0.7, which is referred from Farajzadeh's work [36]. The enthalpies of $CO_2$, oil, and water at different temperatures and pressures can be calculated by using the Winprop module of the CMG software. The energy consumption of the separation of $CO_2$, oil, and water is neglected since the separation process is assumed to take place in a gravity separator vessel.

3.4.3. Results of Energy Analysis

Figure 8 shows the proportion of energy consumed in four major streams, i.e., $CO_2$ capture in the powerplant, $CO_2$ transportation, $CO_2$ and water injection, and $CO_2$ and water reinjection, in Scenario #11. The results show that the respective streams of $CO_2$ capture, $CO_2$ transportation, fluids injection, and fluids reinjection consume 89.1%, 3.1%, 6.3%, and 1.5% of the total energy consumption. In particular, nearly 90% of the energy is consumed in the process of $CO_2$ capture, which means that the most effective way to save energy in the CCUS project is to reduce the energy consumption in $CO_2$ capture.

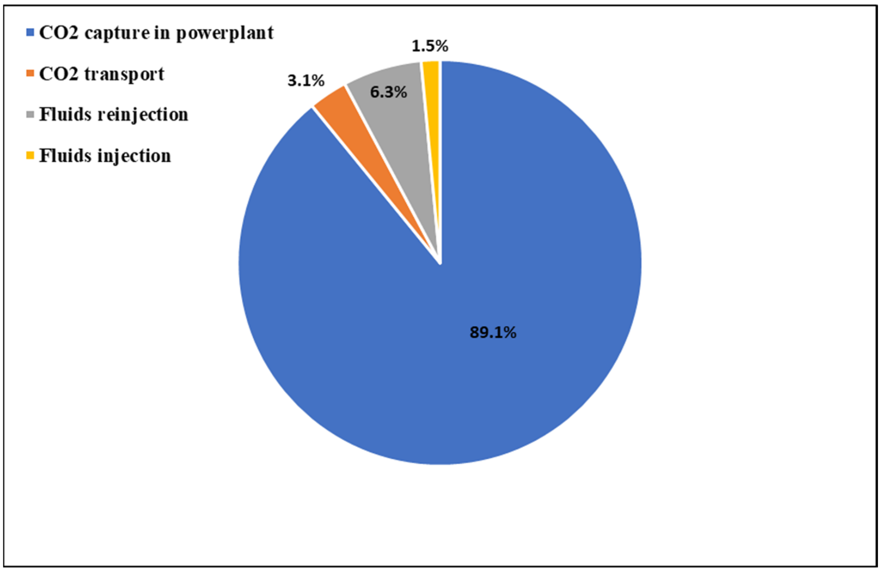


**Figure 8.** The proportions of energy consumption in the CCUS value chain: $CO_2$ capture in a powerplant, $CO_2$ transport, $CO_2$ and water injection, and $CO_2$ and water reinjection.

Figure 9a,b depict the comparison of the net energy gain in Scenario #3 with and without the geothermal energy extraction each year. In this scenario, only the $CO_2$-WAG injection is simulated. It can be seen from Figure 9a that the energy gain is always larger in this scenario with the integration of geothermal energy extraction than that without the integration of the geothermal energy extraction. It can also be found from this figure that without geothermal extraction, a negative energy gain occurs after the seventh year, which means the energy gain from the produced oil is less than the energy consumption in the operation of oil production. This is because the oil production rate declines rapidly with time in the late period of the WAG injection process, which means the only source of energy gain is significantly reduced after the early stage of the WAG injection phase if the geothermal energy extraction is not integrated. Meanwhile, the energy consumptions for oil production including $CO_2$ capture and transportation, $CO_2$ and water injection and reinjection are almost kept the same. As a result, the energy gain cannot cover the energy consumption after the first seven years of oil production. Conversely, a positive energy gain can be achieved in this scenario with geothermal energy extraction (Figure 9a) as geothermal energy extracted from produced $CO_2$, oil, and water compensate the energy loss due to reduced oil production. Figure 9b shows the proportion of respective energy gain from production oil and geothermal energy extraction. At the beginning, the energy gain is mostly entirely from the produced oil. Then the contribution from the geothermal energy increases sharply and surpasses that from the produced oil in the fifth year. From the seventh year, all the energy gains are from geothermal energy. Figure 10 demonstrates the cumulative energy gain in Scenario #11 with and without the integration of the geothermal energy extraction. In this scenario, the entire multi-phase strategy is simulated. It can be seen from this figure that the cumulative net energy gain starts to decrease from the late period of the WAG injection phase and becomes negative in Phase 3. This trend continues until the end of the application of the multi-phase strategy. This is because the energy gain from the produced oil cannot cover the energy consumption for the operation of the $CO_2$-EOR and storage process, which has been stated above. After that, the oil production becomes less and less, and there is even no oil production starting from Phase 2. Thus, the gap between the energy gain and energy consumption becomes larger and larger with time. However, the cumulative net energy gain is always increasing in Phases 1 and 3, and then starts to decrease in Phase 4. It is worth noting that the cumulative net energy gain remains positive during the entire application of the multi-phase strategy. The reason is that the extracted geothermal energy can largely compensate for the reduced energy gain from the produced oil. Thus, there is always a positive net energy gain each year in Phases 1 and 3, which make the cumulative net energy gain keep increasing in these two phases. Phase 4 is the continuing $CO_2$ injection phase, in which there is no energy gain either from the produced oil or the geothermal energy extraction. As a result, the cumulative net energy gain starts to decrease in this phase. However, there is sufficient net energy gain accumulated in Phases 1 and 3 so the cumulative net energy gain stays positive throughout the entire application of the multi-phase strategy.

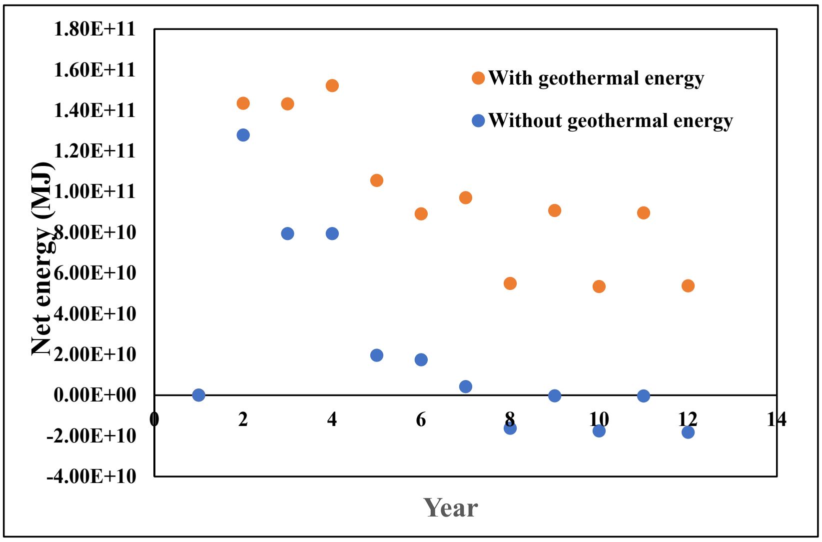


(**a**)

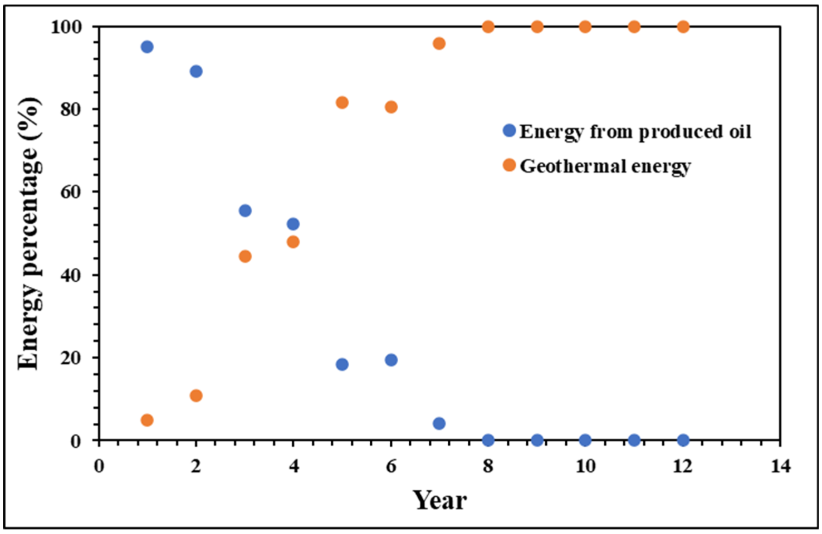


(**b**)

**Figure 9.** The comparisons of (**a**) net energy gain with and without geothermal energy extraction; and (**b**) the percentages of the total energy from the produced oil and geothermal energy extraction.

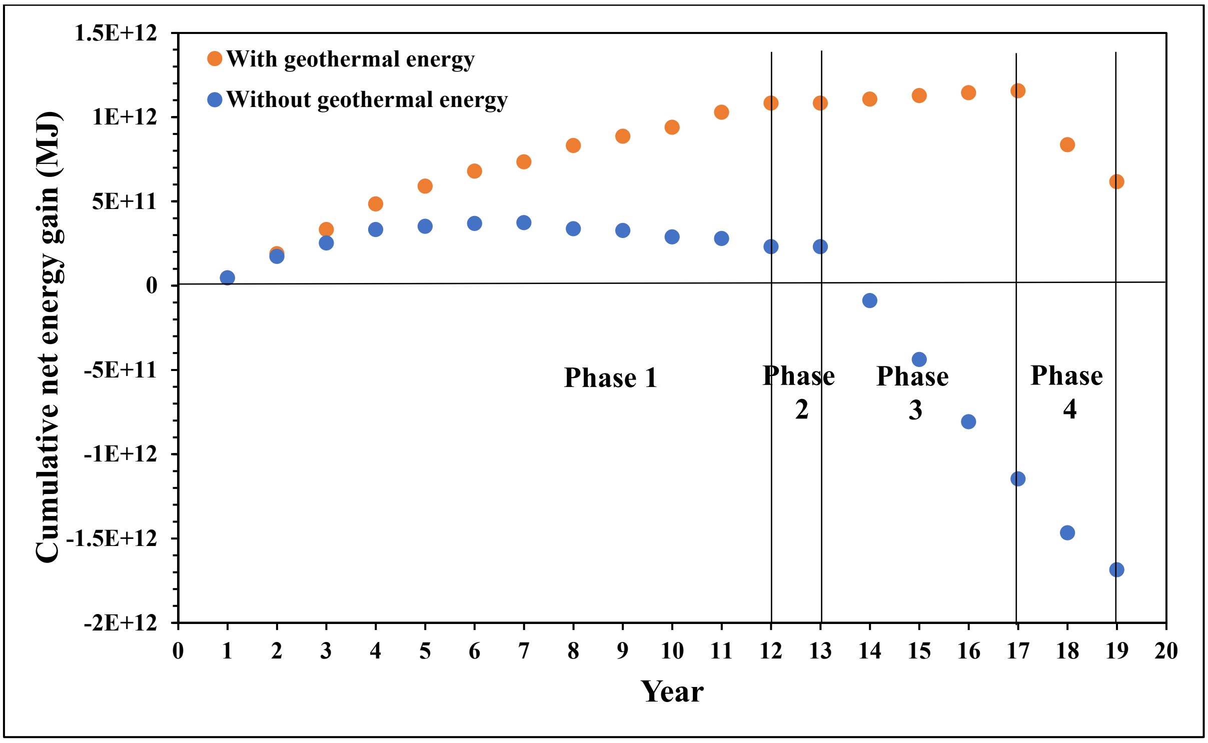


**Figure 10.** The energy analysis result of the cumulative net energy gain throughout the entire application of multi-phase strategy in Scenario #11.

These findings imply that an energy sustainability can be realized by integrating the geothermal energy extraction to counterbalance the insufficient energy gain in the late period of oil production, which could be an attractive incentive for industries to conduct CCUS projects.

*3.5. Limitation and Future Work*

This paper emphasizes the multi-phase strategy and tests the proposed strategy through numerical simulation, which allows extending the utilization life of wells, and using existing wells to convert depleted oil reservoirs into $CO_2$ storage sites as well as producing geothermal energy. We hope that the novel multi-phase strategy together with the idea of converting existing oil and gas reservoir to $CO_2$ storage could accelerate the removal of greenhouse gases in the energy transition by the participation of many small petroleum producers.

Laboratory experiments of real physical models could improve the model and further validate the performance. Although we have planned to conduct experimental work to test some of the performances in the proposed multi-phase strategy on EOR and $CO_2$ storage, there are no physical experimental results available currently to validate the simulation results. However, by numerical simulation, one can first gain insights for optimizing the laboratory experiment or to practically demonstrate a project design in a timely and cost-effective manner for testing new ideas. In addition, the commercial software of CMG has been widely used by industry for various studies to predict or improve the understanding of production performance. The authors believe that the results simulated using CMG in this study should be reliable.

The proposed multi-phase strategy for EOR, $CO_2$ storage, and geothermal production was tested numerically under a small and homogeneous reservoir model in this study. Thus, some of the optimal operational parameters obtained from this model may not be directly applicable to a real reservoir complex in practice. For example, in real situations, the best water–$CO_2$ slug ratio may not be 1:1 and the shut in period may not be exactly one year. However, the qualitative conclusions, such as the existence of an optimum water–$CO_2$ slug ratio and the multi-phase strategy can definitely increase the amount of $CO_2$ storage.

In this study, we assumed that the geothermal energy resources from the produced fluids can be utilized to offset some energy needs in the operation site and use the net energy values of the products, such as oil and heat, while in the energy balance calculation, we did not consider the extra energy needed or energy lost in the energy conversion before the utilization. This needs to be addressed in a future study.

## 4. Conclusions

In this paper, a multi-phase strategy is proposed to utilize $CO_2$ to enhance the oil recovery, store $CO_2$ to reduce the greenhouse gas emissions, and use the by-product of geothermal energy from produced fluids to offset GHG emissions at the operation site. A series of scenarios are simulated to validate the effectiveness and efficiency of the newly proposed multi-phase strategy.

The following conclusions can be drawn from this study.

- The water-alternating-gas (WAG) injection, as the first phase of the multi-phase strategy, is implemented to recover oil and store $CO_2$ at the same time. It is found that the scenario with the water–$CO_2$ slug ratio of 1:1 has the highest oil recovery rate and $CO_2$ utilization ratio in comparison with those with the water–$CO_2$ slug ratios of 3:1 and 1:3.
- The amount of $CO_2$ storage is doubled by applying the new multi-phase strategy in comparison to that by the WAG injection process alone. This indicates, on the one hand, the new multi-phase strategy is effective and efficient in $CO_2$ storage. On the other hand, the existing wells after the WAG injection process can be used for the purpose of $CO_2$ storage, which can save significant capital investment in well drilling.
- The $CO_2$ injection rate in the third and fourth phases does not appreciably affect the $CO_2$ storage amount when the multi-phase strategy is applied, which means that the $CO_2$ storage process can be accelerated by increasing the $CO_2$ injection rate without impairing the ultimate amount of $CO_2$ storage.
- Lastly, from the results of energy analysis, a net energy gain can be achieved when the geothermal energy extraction is integrated with the newly proposed multi-phase strategy. Thus, the multi-phase strategy is sustainable from the energy aspect, though its economic feasibility remains to be studied.

**Author Contributions:** J.Y.: Conceptualization, Draft, Analysis; W.Y.: conceptualization and analysis; X.P.: conceptualization and analysis; Z.C.: funding and revision; Y.G.: revision. All authors have read and agreed to the published version of the manuscript.

**Funding:** This research is funded by OERD 331404 of Natural Resources Canada.

**Data Availability Statement:** The data presented in this study are available on request from the corresponding author.

**Acknowledgments:** This is an output from Geoscience for New Energy Program of Natural Resources Canada. The Office of Energy Research and Development of Natural Resource Canada funded this study.

**Conflicts of Interest:** The authors declare no conflict of interest.

## References

1. Obobisa, E.S. Achieving 1.5 °C and net-zero emissions target: The role of renewable energy and financial development. *Renew. Energy* **2022**, *188*, 967–985. [CrossRef]
2. Environment and Climate Change Canada. Greenhouse Gas Emissions, Canadian Environmental Sustainability Indicators. 2022, ISBN 978-0-660-421193. Available online: https://www.canada.ca/en/environment-climate-change/services/environmental-indicators/greenhouse-gas-emissions.html (accessed on 14 April 2023).

3. Peng, X.; Chen, Z.; Zeng, F.; Yuan, W.; Yao, J.; Hu, K. Feasibility of Carbon Storage in Kirby Depleted Shallow Gas Fields: A Numerical and Statistical Analysis. In Proceedings of the SPE Canadian Energy Technology Conference and Exhibition, Calgary, AB, Canada, 15–16 March 2023. [CrossRef]
4. Saira; Janna, F.; Le-Hussain, F. Effectiveness of modified $CO_2$ injection at improving oil recovery and $CO_2$ storage—Review and simulations. *Energy Rep.* **2020**, *6*, 1922–1941. [CrossRef]
5. Bello, A.; Dorhjie, D.B.; Ivanova, A.; Cheremisin, A. A Numerical Study of the Influence of Rock Mineralization on CO2 Storage. In Proceedings of the Gas & Oil Technology Showcase and Conference, Dubai, United Arab Emirates, 13–15 March 2023. [CrossRef]
6. Ahmadi, M.A.; Pouladi, B.; Barghi, T. Numerical Modeling of $CO_2$ Injection Scenarios in Petroleum Reservoirs: Application to $CO_2$ Sequestration and EOR. *J. Nat. Gas Sci. Eng.* **2016**, *30*, 38–49. [CrossRef]
7. Bello, A.; Ivanova, A.; Cheremisin, A. A Comprehensive Review of the Role of $CO_2$ Foam EOR in the Reduction of Carbon Footprint in the Petroleum Industry. *Energies* **2023**, *16*, 1167. [CrossRef]
8. Ravagnani, A.G.; Ligero, E.; Suslick, S. $CO_2$ sequestration through enhanced oil recovery in a mature oil field. *J. Pet. Sci. Eng.* **2009**, *65*, 129–138. [CrossRef]
9. Zhang, L.; Ren, B.; Huang, H.; Li, Y.; Ren, S.; Chen, G.; Zhang, H. $CO_2$ EOR and storage in Jilin oilfield China: Monitoring program and preliminary results. *J. Pet. Sci. Eng.* **2015**, *125*, 1–12. [CrossRef]
10. Chen, H.; Yang, S.; Xue, Z.; Wang, Z.; Lv, S.; Hu, W.; Lei, H.; Qiu, Z. Experimental study on seismic response during $CO_2$ sequestration with different phase state. *J. Energy Inst.* **2016**, *89*, 30–39. [CrossRef]
11. Agada, S.; Geiger, S.; Doster, F. Wettability, hysteresis and fracture–Matrix interaction during $CO_2$ EOR and storage in fractured carbonate reservoirs. *Int. J. Greenh. Gas Control* **2016**, *46*, 57–75. [CrossRef]
12. Azzolina, N.A.; Nakles, D.V.; Gorecki, C.D.; Peck, W.D.; Ayash, S.C.; Melzer, L.S.; Chatterjee, S. $CO_2$ storage associated with $CO_2$ enhanced oil recovery: A statistical analysis of historical operations. *Int. J. Greenh. Gas Control* **2015**, *37*, 384–397. [CrossRef]
13. Rezk, M.G.; Foroozesh, J.; Zivar, D.; Mumtaz, M. $CO_2$ storage potential during $CO_2$ enhanced oil recovery in sandstone reservoirs. *J. Nat. Gas Sci. Eng.* **2019**, *66*, 233–243. [CrossRef]
14. Hosseininoosheri, P.; Hosseini, S.; Lopez, V.N.; Lake, L. Impact of field development strategies on $CO_2$ trapping mechanisms in a $CO_2$-EOR field: A case study in the permian basin (SACROC unit). *Int. J. Greenh. Gas Control* **2018**, *72*, 92–104. [CrossRef]
15. Sacuta, N.; Daly, D.; Botnen, B.; Worth, K. Communicating about the Geological Storage of Carbon Dioxide—Comparing Public Outreach for $CO_2$ EOR and Saline Storage Projects. *Energy Procedia* **2017**, *114*, 7245–7259. [CrossRef]
16. Cho, J.; Min, B.; Kwon, S.; Park, G.; Lee, K.S. Compositional modeling with formation damage to investigate the effects of $CO_2$–CH4 water alternating gas (WAG) on performance of coupled enhanced oil recovery and geological carbon storage. *J. Pet. Sci. Eng.* **2021**, *205*, 108795. [CrossRef]
17. Lei, H.; Yang, S.; Zu, L.; Wang, Z.; Li, Y. Oil Recovery Performance and $CO_2$ Storage Potential of $CO_2$ Water-Alternating-Gas Injection after Continuous $CO_2$ Injection in a Multilayer Formation. *Energy Fuels* **2016**, *30*, 8922–8931. [CrossRef]
18. Cui, G.; Zhang, L.; Tan, C.; Ren, S.; Zhuang, Y.; Enechukwu, C. Injection of supercritical $CO_2$ for geothermal exploitation from sandstone and carbonate reservoirs: $CO_2$-water-rock interactions and their effects. *J. $CO_2$ Util.* **2017**, *20*, 113–128. [CrossRef]
19. Majorowicz, J.; Grasby, S.E. Deep geothermal energy in Canadian sedimentary basins vs. Fossils based energy we try to replace—Exergy [KJ/KG] compared. *Renew. Energy* **2019**, *141*, 259–277. [CrossRef]
20. Kumari, W.; Ranjith, P.; Perera, M.; Shao, S.; Chen, B.; Lashin, A.; Arifi, N.; Rathnaweera, T. Mechanical behaviour of Australian Strathbogie granite under in-situ stress and temperature conditions: An application to geothermal energy extraction. *Geothermics* **2017**, *65*, 44–59. [CrossRef]
21. Brown, D.W. A hot dry rock geothermal energy concept utilizing supercritical $CO_2$ instead of water. In Proceedings of the twenty-fifth workshop on geothermal reservoir engineering, Stanford, CA, USA, 24–26 January 2020.
22. Pruess, K. Enhanced geothermal systems (EGS) using $CO_2$ as working fluid—A novel approach for generating renewable energy with simultaneous sequestration of carbon. *Geothermics* **2006**, *35*, 351–367. [CrossRef]
23. Cui, G.; Ren, S.; Zhang, L. Effects of Rock-Fluid Interaction and Water Back Flow on Heat Mining Efficiency of Geo-thermal Development via Carbon Dioxide Injection. *J. Chem. Eng. Chin. Univ.* **2016**, *30*, 1043–1052. [CrossRef]
24. Cui, G.; Zhang, L.; Ren, B.; Enechukwu, C.; Liu, Y.; Ren, S. Geothermal exploitation from depleted high temperature gas reservoirs via recycling supercritical $CO_2$: Heat mining rate and salt precipitation effects. *Appl. Energy* **2016**, *183*, 837–852. [CrossRef]
25. Pruess, K. On production behavior of enhanced geothermal systems with $CO_2$ as working fluid. *Energy Convers. Manag.* **2008**, *49*, 1446–1454. [CrossRef]
26. Huang, C.-J.; Hsieh, J.-C.; Lin, D.T.W.; Kuo, J.-K.; Hu, Y.-C. The experimental study of heat extraction of supercritical $CO_2$ in the geothermal reservoir. *MATEC Web Conf.* **2016**, *60*, 4010. [CrossRef]
27. Hsieh, J.; Lin, D.T.; Wei, C.; Huang, H. The Heat Extraction Investigation of Supercritical Carbon Dioxide Flow in Heated Porous Media. *Energy Procedia* **2014**, *61*, 262–265. [CrossRef]
28. Randolph, J.B.; Saar, M.O. Coupling carbon dioxide sequestration with geothermal energy capture in naturally permeable, porous geologic formations: Implications for $CO_2$ sequestration. *Energy Procedia* **2011**, *4*, 2206–2213. [CrossRef]
29. Yan, S.; Wang, F.G.; Yang, Y.L.; Feng, G.H. Integration of Carbon Geological Storage and Geothermal Energy Development in Low-Permeability Reservoirs. *Appl. Mech. Mater.* **2013**, *448–453*, 4350–4357. [CrossRef]
30. Garapati, N.; Randolph, J.B.; Valencia, J.L.; Saar, M.O. $CO_2$-Plume Geothermal (CPG) Heat Extraction in Multi-layered Geologic Reservoirs. *Energy Procedia* **2014**, *63*, 7631–7643. [CrossRef]

31. Adams, B.M.; Kuehn, T.H.; Bielicki, J.M.; Randolph, J.B.; Saar, M.O. On the importance of the thermosiphon effect in CPG ($CO_2$ plume geothermal) power systems. *Energy* **2014**, *69*, 409–418. [CrossRef]
32. Exploration Staff, Chevron Standard Ltd. The geology, geophysics and significance of the nisku reef discoveries, west pembina area, Alberta, Canada. *Bull. Can. Pet. Geol.* **1979**, *27*, 326–359. [CrossRef]
33. Yao, J.; Gu, Y. A new experimental method for measuring the bubble-point pressures of the light crude oil-$CO_2$ system at different $CO_2$ concentrations. *Fuel* **2021**, *311*, 122526. [CrossRef]
34. Chen, Z.; Zhou, Y.; Li, H. A Review of Phase Behavior Mechanisms of $CO_2$ EOR and Storage in Subsurface Formations. *Ind. Eng. Chem. Res.* **2022**, *61*, 10298–10318. [CrossRef]
35. Sánchez, Y.A.C.; de Oliveira, S. Exergy analysis of offshore primary petroleum processing plant with $CO_2$ capture. *Energy* **2015**, *88*, 46–56. [CrossRef]
36. Farajzadeh, R.; Eftekhari, A.A.; Dafnomilis, G.; Lake, L.; Bruining, J. On the sustainability of $CO_2$ storage through $CO_2$-Enhanced oil recovery. *Appl. Energy* **2020**, *261*, 114467. [CrossRef]
37. Plasynski, S.; Chen, Z. *Review of $CO_2$ Capture Technologies and Some Improvement Opportunities*; American Chemical Society: Washington, DC, USA, 2000.